Synchrotron photoemission study of CO chemisorption on Cr(110)

Neal D. Shinn
Surface Science Division, National Institute of Science and Technology, Gaithersburg, Maryland 20899
*and Sandia National Laboratories (Division 1134), Albuquerque, New Mexico 87185**
(Received 17 May 1988; revised manuscript received 22 August 1988)

Angle-integrated ultraviolet photoemission studies of carbon monoxide chemisorption on Cr(110) confirm the sequential population of two electronically inequivalent molecular binding states (α_1-CO and α_2-CO) at 90 K. These are distinguished by differences in the CO 4σ binding energies ($\Delta E_B = 0.8$ eV) and photoemission cross sections. Work-function measurements indicate that the surface dipole moment associated with α_1-CO is significantly less than that for α_2-CO. CO/O interaction data exhibit oxygen-induced α_1-CO site blocking and α_1-CO$\rightarrow\alpha_2$-CO binding mode conversion. These results support current models for the CO binding geometries on Cr(110) and related binding states on Fe (100) and Mo(100).

I. INTRODUCTION

Ultraviolet photoelectron spectroscopy is a well-established and powerful tool for determining both the electronic structure and the molecular orientation of carbon monoxide chemisorbed on single-crystal transition-metal surfaces.[1-3] With the availability of tunable, linearly polarized ultraviolet synchrotron radiation, detailed studies of the photoionization cross sections and resonant photoemission processes are also possible. Together, these are important contributions to our understanding of correlations among the CO-metal bonding, the surface electronic properties, and the observed CO surface chemistry.

The discovery of a new class of chemisorbed carbon monoxide on Cr(110),[4] Fe(111),[5] Fe(100),[6-8] and Mo(100) (Ref. 9) single-crystal surfaces, i.e., adsorbed CO species that are *not* direct analogs to common transition-metal carbonyl complexes,[10] provides new opportunities to further understand the mechanism and dynamics of catalytic CO dissociation, and the role of the surface electronic structure and morphology in this process. The Fe(111) case is most like CO chemisorption on other metal surfaces, since the surface morphology allows the π system of a terminally bonded CO(ads) to interact strongly with surrounding iron atoms, thereby increasing the back-bonding and decreasing the CO stretching frequency. On the three other surfaces, a molecular CO binding state has been found which (1) is populated prior to, or simultaneously with, terminally bonded CO chemisorption states, (2) exhibits a reduced C-O stretching frequency in the range of 1100–1500 cm^{-1}, and (3) is implicated as an intermediate or precursor to CO dissociation.

These observations have lead to proposals[4,6-8] that the bonding of these dissociation intermediates to their respective metal surfaces involves a greater overlap of the CO frontier orbitals—particularly the CO π system—with the substrate metal orbitals than can be obtained if only the carbon end of the molecule is in close proximity with the surface. This chemisorption bonding is inadequately described by the synergistic backbonding in the Blyholder[11] model. Consequently, atypical local CO bonding geometries reflecting the Cr(110), Fe(100), and Mo(100) surface morphologies might be expected. On the bcc (100) plane, the C_{4v} symmetric hollow site enables the CO molecule to be embedded partially among the metal atoms,[6-8] whereas on the close-packed bcc (110) plane, this would be sterically prevented. However, a tilted geometry in the C_{2v} symmetric hollow site ("hourglass" site) on the (110) plane could facilitate the enhanced π-orbital overlap.[4] The electronic structure differences implied by this hypothesis motivated the present ultraviolet photoemission study of CO bonding to Cr(110).

On Cr(110) below $\sim$150 K, the CO dissociation intermediate, designated as the α_1-CO molecular binding state, was found to saturate with the formation of an ordered $c(4\times2)$ overlayer at a coverage (Θ_{CO}) of $\frac{1}{4}$ monolayer; only after $\Theta_{CO} > 0.25$ do CO molecules adsorb in the second binding state (α_2-CO). [One monolayer (ML), $\Theta = 1$, is defined as the number density of surface chromium atoms on the ideal Cr(110) plane, 1.705×10^{15} cm^{-2}.] Total CO saturation coverage is achieved at $\Theta_{CO}\approx0.35$ monolayers.[4] In order to explain α_1-CO vibrational frequencies in the 1150 $cm^{-1}\rightarrow$1330 cm^{-1} range, as measured by high-resolution electron-energy-loss spectroscopy (HREELS), and a lack of CO^+ or O^+ ions in electron-stimulated-desorption ion angular distribution (ESDIAD) measurements,[4] this α_1-CO state was proposed to consist of CO molecules strongly tilted or "lying down" on the Cr(110) surface in surface hollow sites of C_{2v} symmetry such that both the carbon and the oxygen atoms are coordinated to the metal; such a configuration has been postulated by others[12,13] as a plausible transition state for CO dissociation on metal surfaces in general. This model is shown in Fig. 1. The important aspect of this α_1-CO model is not the exact geometry of the molecule but the idea that *all* of the CO frontier orbitals (4σ, 1π, and 5σ) would be perturbed by their interaction with the chromium surface. A low-symmetry bonding

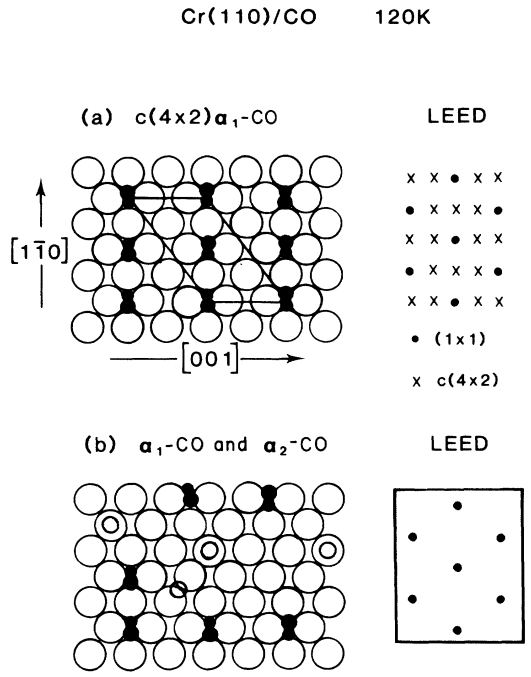

FIG. 1. Models for (a) ordered $c(4\times2)\alpha_1$-CO overlayer, and (b) disordered mixed overlayer for $\Theta_{CO} > 0.25$ ML.

configuration might also serve to break the degeneracy of the 1π orbitals. It should be noted that a reduced yield for electron-stimulated desorption (ESD) of positive ions does *not* require a tilted or lying down bonding geometry; this would be a sufficient but not necessary condition to extinguish the positive ion signal, since the desorbed CO^+ or O^+ ion would be recaptured by its image charge.[14]

This paper reports CO-coverage-, photon-energy-, and collection-geometry-dependent angle-integrated photoemission data, and work-function measurements for molecular CO chemisorption at 90 K, expanding upon a previously published brief report,[15] and new data for dissociation and CO/O interaction studies. The experimental procedures and results are described in Secs. II and III, respectively, followed by a discussion in Sec. IV of plausible models and criteria for future experiments to test these models.

II. EXPERIMENT

Ultraviolet photoelectron spectroscopic (UPS) measurements using synchrotron radiation were performed on the surface science beamline[16] at the Synchrotron Ultraviolet Radiation Facility (SURF-II) synchrotron storage ring located at the National Institute of Standards and Technology. The ion and titanium-sublimation pumped ultrahigh vacuum (UHV) chamber (base pressure 2×10^{-11} Torr) is equipped with a double-pass cylindrical mirror electron-energy analyzer (CMA) with a coaxial electron gun, rear-viewing optics for low-energy electron diffraction (LEED) and ESDIAD, ion sputter gun, quadrupole mass spectrometer, and a moveable microcapillary array gas doser. CO exposures were made using either the doser or by backfilling the UHV chamber, with no measurable spectroscopic differences.

Linearly polarized radiation from SURF-II was dispersed by a 6-m toroidal grating monochromator[17] (TGM) and was incident upon the Cr(110) crystal in a plane containing the Cr [110] and [001] aximuths and the CMA axis. With respect to the crystallographic coordinate system, the component of the photon polarization vector, **A**, parallel to the surface lies along the crystallographic [001] direction.

Figure 2 illustrates the experimental layout and the definition of the laboratory angular coordinate system (θ_{lab}) used in the following sections. $\theta_{lab}=90°$ corresponds to normal incidence (*s* polarization) whereas $\theta_{lab}=0°$ corresponds to grazing incidence. Because the CMA position is fixed with respect to both the incident photon direction and its polarization vector (**A**), rotation of the sample manipulator (which is a rotation of the crystal about the Cr [1$\bar{1}$0] axis) results in coupled variations in (1) the photon incidence angle, (2) the effective polarization vector[18,19] ($\mathbf{A}_{eff}$) at the chromium surface, and (3) the photoelectron detection geometry and solid angle. Thus these angle-integrated photoemission data average over a solid angle in reciprocal space which varies with the selected θ_{lab}. Most of the data presented in this paper were obtained at $\theta_{lab}=42°$, which included photoelectron trajectories from normal emission to near grazing, since this was found to be the optimal configuration within the experimental constraints for distinguishing between the two molecular binding states. Data obtained at other θ_{lab} values are summarized in Sec. III D.

The crystal preparation and *in situ* Cr(110) surface cleaning procedure have been described previously.[4] Auger-electron spectroscopy (AES) and LEED were used to verify the initial surface cleanliness and the absence of surface faceting or reconstruction. As in the vibra-

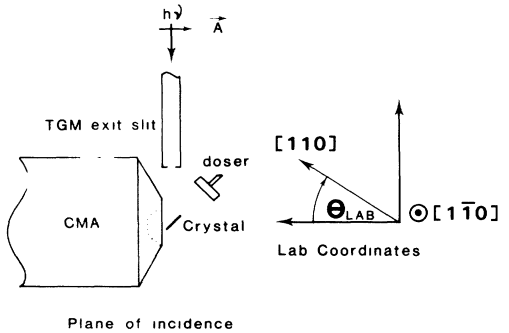

FIG. 2. (Left) Configuration of the experiment viewed in the plane of photon incidence, which contains the chromium [110] (surface normal) and [001] azimuths, the polarization vector, **A**, of the linearly polarized synchrotron radiation, the CMA axis, and the center of the microcapillary array doser when moved into position. (Right) The angle θ_{lab}, defined as the angle between the chromium surface normal and the cylindrical axis of the CMA, is varied by rotation of the sample manipulator. UPS spectra including normal emission were taken at $\theta_{lab}=42°$.

tional (HREELS) and electron-stimulated-desorption (ESDIAD) experiments using the same Cr single crystal, the residual carbon impurity level was found to be less than 5% of a monolayer (determined by the carbon-to-chromium AES peak height ratio). The residual surface oxygen contamination was estimated by a comparison of the integrated UPS valence-band oxygen intensity on the sputter-annealed and deliberately oxygen-dosed surfaces, using the $p(4\times2)$O overlayer as an oxygen coverage calibration point.[20] The sputter-annealed Cr(110) surface typically had less than 0.03 monolayers of residual atomic oxygen, which had only a minimal effect on molecular binding modes.[21]

III. RESULTS

A. Initial surface characterization

Prior to obtaining the CO chemisorption data, the UPS spectra of the clean Cr(110) surface were recorded to identify intrinsic features which appear at the CO valence orbital binding energies. Figures 3 and 4 show clean Cr(110) spectra for $\theta_{lab}=42°$. These spectra have been normalized for the incident radiation flux from SURF-II and displaced vertically for clarity. Two weak features, indicated by dashed lines and solid arrows are evident in the low-photon-energy data (Fig. 3), while the intense chromium $M_{2,3}VV$ Auger transition,[22] at $\sim$36 eV kinetic energy, and resonating two-electron satellite peak, at $\sim$6 eV binding energy,[23–25] dominate the spectra for $h\nu$ above the Cr $3p$ threshold[26,27] at 42.3 eV (Fig. 4).

The two weak features in Fig. 3 are clearly an Auger transition (dashed line) and a second-order photoemission feature (arrow) as indicated by their binding energy variations with photon energy. A simple calculation shows that the second-order UPS peak is due to the Cr $3p$ level at a binding energy of 42.3 eV. The Auger transition could be a carbon LVV transition although its intensity is

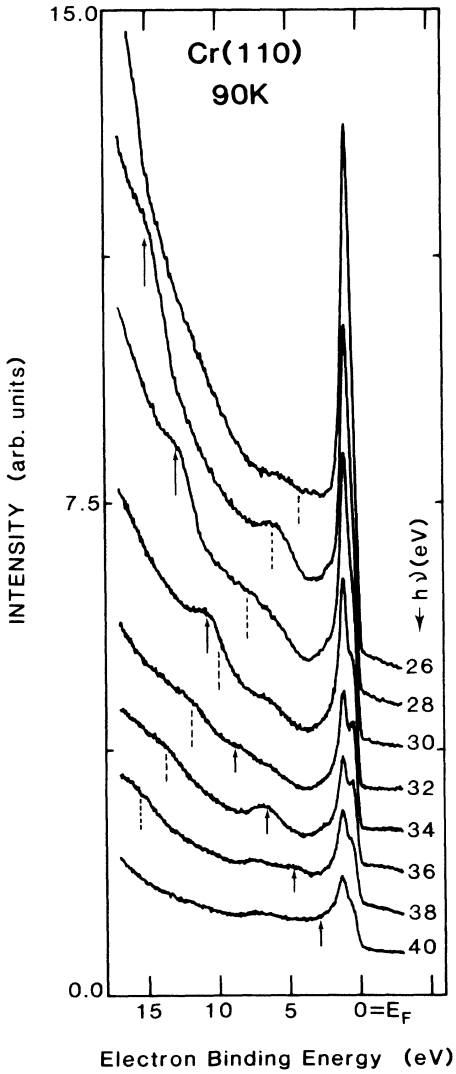

FIG. 3. UPS data taken at $\theta_{lab}=42°$ with increasing photon energy, for the sputter-annealed Cr(110) surface. Solid arrows and dashed markers below the spectra indicate the positions of the second-order Cr $3p$ photoemission peak and an Auger transition, respectively.

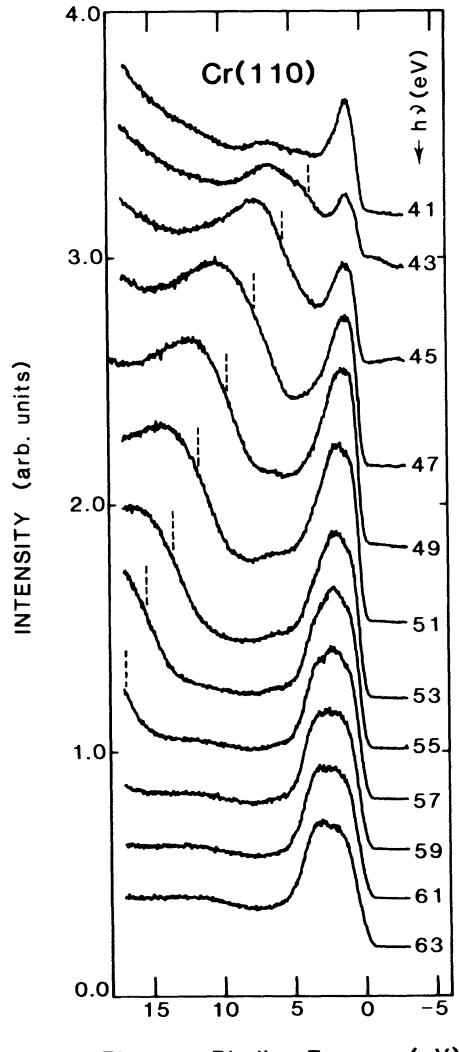

FIG. 4. UPS data taken at $\theta_{lab}=42°$ with higher energy photons for the sputter-annealed Cr(110) surface. Dashed line indicates the position of the $\sim$36-eV Cr $M_{23}VV$ Auger transition.

greater than would be expected based upon the low-carbon *KLL* transition intensity on the same surface. To simplify the interpretation of the CO-coverage–dependent data, the above considerations show that photon energies of less than 26 eV, ~40 eV, or greater than 52 eV should be used. In these cases, the entire valence band is uncongested and the inelastic background can be fit numerically by a smooth function. Due to the CO 4σ shape resonance[28,29] near $h\nu = 36$ eV and the availability of He-II (40.8 eV) UPS data for CO on numerous transition metals for comparisons, a photon energy of 40 eV was used for CO-coverage–dependent experiments.

B. CO-coverage dependence

Significant differences in the electronic structure of α_1-CO and α_2-CO are unmistakable in the coverage-dependent UPS data alone. Figure 5 shows a series of spectra for the α_1-CO binding state obtained with 40-eV photons in the standard geometry. In Fig. 5(a), the weak peak at $E_B = 7$ eV seen for the sputter-annealed surface is attributed to a combination of the (1) two-electron Cr satellite intrinsic to the Cr(110) surface[23–25] and (2) oxygen $2p$ intensity from the residual surface oxygen coverage of $\Theta_0 < 0.05$ monolayers. The addition of up to 1.0 L CO [1 langmuir (L) $= 10^{-6}$ Torr sec] in increments of 0.2 L leads to a broad peak at 7–8 eV, a weak peak at 11.6±0.1 eV, and an increase in the density of states at the bottom of the chromium $3d$ band. [CO-induced changes in the Cr(110) $3d$ valence bands were seen at other experimental geometries where $\theta_{lab} \neq 42°$ as well.] The broad peak extending over $7 < E_B < 8$ eV is assigned to the perturbed CO 5σ and 1π molecular orbitals, and the 11.6-eV peak is assigned to the CO 4σ level. These assignments are based upon the measured photon-energy dependences (see Sec. III E), data obtained at various collection geometries (Sec. III D), and the UPS peak assignments for other transition-metal CO systems.[2,3,30] However, the use of these one electron labels for the unperturbed CO molecular orbitals is, strictly speaking, inaccurate since *all* of the valence orbitals of a dissociation intermediate on Cr(110) would be expected to be significantly perturbed and perhaps symmetry mixed with metal orbitals by direct interactions with the metal surface.

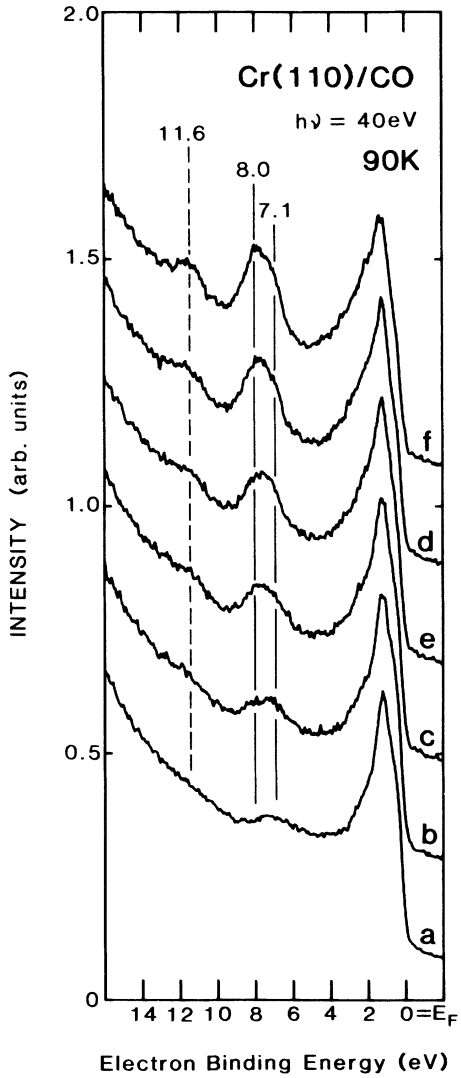

FIG. 5. CO-coverage–dependent data obtained at $\theta_{lab} = 42°$. CO exposures are (a) 0.0 L, (b) 0.2 L, (c) 0.4 L, (d) 0.6 L, (e) 0.8 L, and (f) 1.0 L. 1 L $= 10^{-6}$ Torr sec. Spectra have been normalized to the incident photon flux, smoothed with a three-point routine and vertically displaced in fixed increments. Positions of the three Gaussian components used to fit the direct photoemission peaks (see text) are shown by the vertical lines.

Based upon the earlier HREELS and stimulated desorption results,[4,14] CO exposures above ~0.8 L should result in the population of the α_2-CO mode, which was modeled by terminally bonded CO aligned roughly with the [110] surface normal direction. The $\theta_{lab} = 42°$ experimental configuration is optimal, within the experimental constraints of this angle-integrated experiment, for strong α_2-CO 4σ photoemission intensity[3,31] if this model is correct. Figure 6 shows representative spectra from 1 L CO to saturation at ~3 L CO, demonstrating the sequential population of a second molecular binding mode which is inequivalent to the initially populated α_1-CO mode. The most pronounced spectral difference is the peak at 10.8 eV binding energy which increases in intensity with CO exposure to dominate the spectrum at saturation. This is consistent with an α_2-CO molecule oriented normal to the surface. Because the present apparatus is not an angle-resolved instrument, data from which a definitive determination of the molecular orientation could not be obtained. More importantly, the substantial binding-energy difference between the α_1-CO 4σ level at 11.6 eV and that of α_2-CO at 10.8 eV demonstrates that the two adsorbed CO species are *electronically inequivalent* and must differ in their bonding to the Cr surface.

Each spectrum in the adsorption series of Figs. 5 and 6 has been analyzed numerically by first removing a polynomial functional fit to the inelastic electron background at five points and then fitting Gaussian peak shapes to the data. No attempt was made to deconvolute the instrumental broadening from the spectra. Figure 7(a) shows a sample fit to an α_1-CO UPS spectrum after background subtraction. For low CO coverages, two Gaussians were used to fit the broad $(1\pi + 5\sigma)$ peak and were chosen to be of equal full width at half maximum (FWHM). The

best fit for the series was a doublet at 7.2±0.1 and 8.0±0.1 eV, both with a FWHM of 1.35±0.5 eV. The present data are insufficient to (1) justify the use of additional Gaussians or (2) extract a separate FWHM for each component. A single Gaussian at 11.6±0.1 eV was sufficient to fit the α_1-CO 4σ peak. In no data was the α_1-CO 4σ peak asymmetric, which would have indicated multiple overlapping components, like the combination $(1\pi+5\sigma)$ peak, or additional two-electron (shake-up) final states.[32] However, the measured single Gaussian FWHM of 1.50±0.05 eV was even greater than that of the 5σ or 1π components, which is unexpected for a largely nonbonding orbital[33] spatially localized on the oxygen end of the adsorbed CO. This point will be considered further in the Discussion section.

After the onset of α_2-CO (Fig. 5), a fourth Gaussian component at 10.8±0.1 eV was added, but with a FWHM of only 1.0 eV [Fig. 7(b)]. Although the population of the α_2-CO binding state is expected to add two additional components to the $(1\pi+5\sigma)$ combination peak, the present data are insufficient to extract a total of four independent Gaussians, of unknown position and intensities, from one broad spectral feature. Detailed angle-resolved UPS data, recorded at configurations to measure α_1 or α_2 features selectively,[34] might be able to separate these interfering components (see Sec. IV). Figure 8 shows the extracted component intensities as a function of CO exposure for the data of Figs. 5 and 6. Because the initial α_1-CO sticking probability is ~0.9 (decreasing with $\Theta_{\alpha_1\text{-CO}}$) and that of α_2-CO ~0.3, the total CO coverage at 1 and 3 L are approximately 0.25 and 0.35 monolayers, respectively.[4] The 4σ intensity distributions for the α_1 and α_2 binding modes, at 11.6 and 10.8 eV respec-

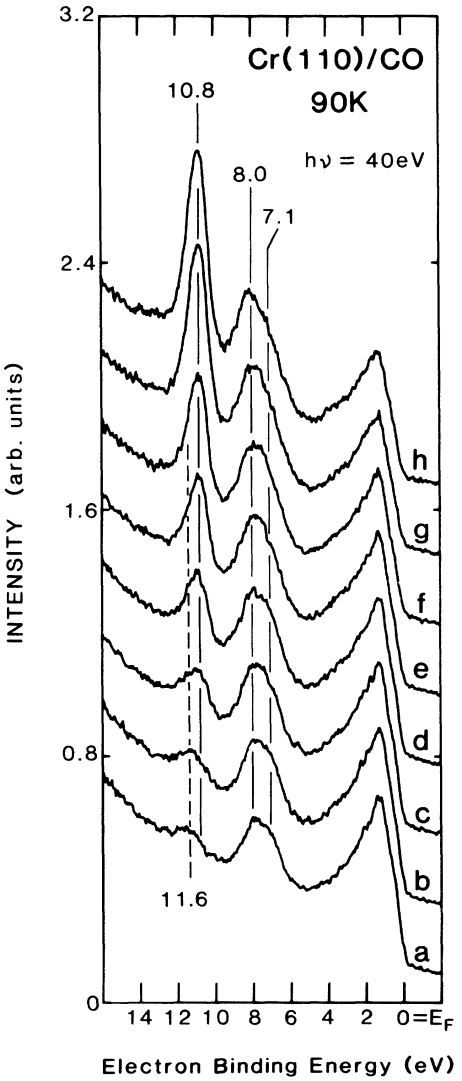

FIG. 6. CO-coverage-dependent data obtained at $\theta_{lab}=42°$ for exposures of (a) 1.0 L, (b) 1.2 L, (c) 1.4 L, (d) 1.6 L, (e) 1.8 L, (f) 2.0 L, (g) 2.6 L, and (h) 3.0 L. Spectra have been normalized to the incident photon flux, smoothed by a three point routine and vertically displaced in fixed increments. Vertical lines indicate binding-energy positions for the four Gaussian components used to fit these spectra (see text). Numerical intensity scale is directly comparable to that of Fig. 4.

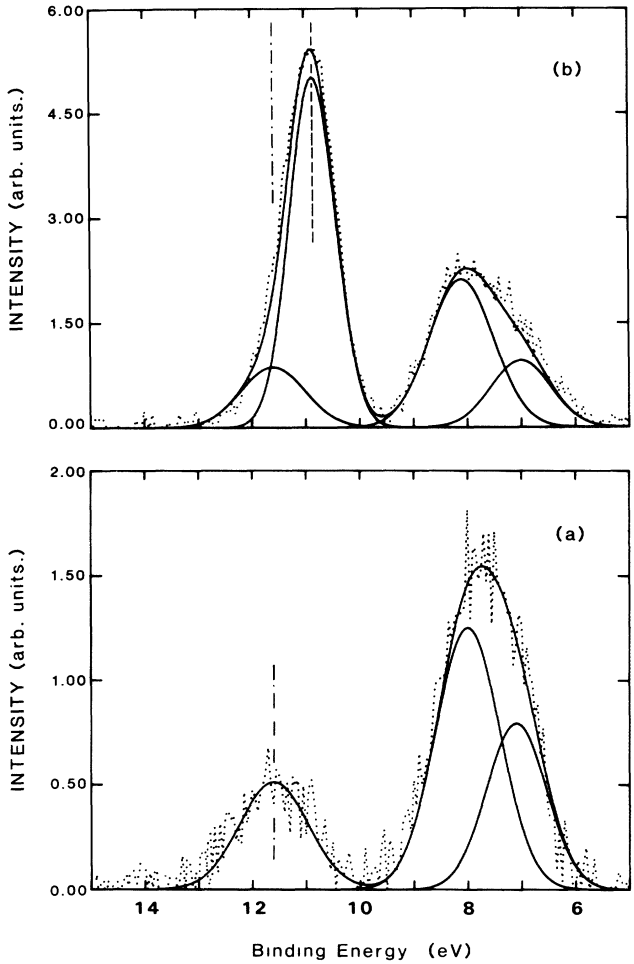

FIG. 7. Sample spectra after subtraction of spline background function and fitting with Gaussian peak shapes: (a) 0.8 L CO exposure (α_1-CO only) and (b) 3.0 L CO exposure (saturation α_1-CO and α_2-CO). Dotted lines are unsmoothed data and solid lines are Gaussian fits with the individual components also shown. Intensity scales (in arbitrary units) are directly comparable. See text for fitting parameters.

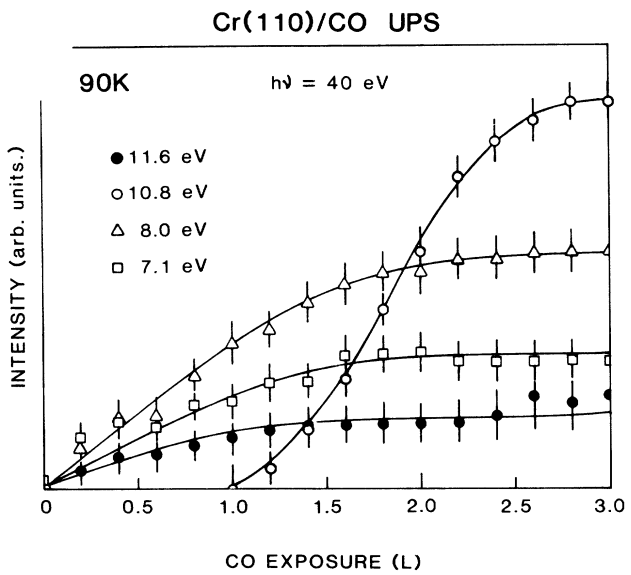

FIG. 8. Intensity distributions for CO-induced UPS peaks as a function of total CO exposure obtained at $\theta_{lab}=42°$.

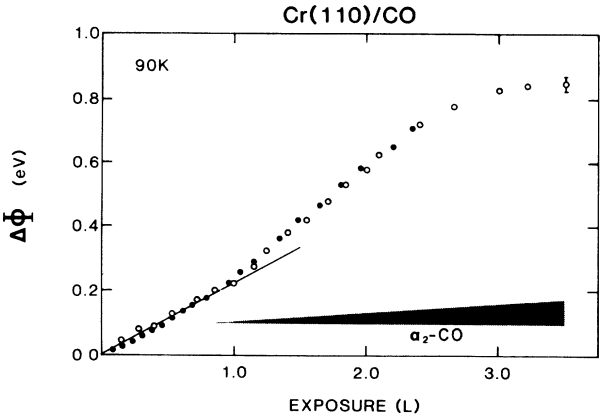

FIG. 9. Work-function change, measured by the secondary electron-energy cutoff, as a function of CO exposure at 90 K. Different symbols refer to different experimental runs. Solid line indicates nearly linear increase of Φ during the α_1-CO adsorption stage and the shaded region indicates the appropriate exposures for the filling of the α_2-CO binding state.

tively, follow the exposure-dependent vibrational intensity distributions published previously[4] with one exception: whereas the vibrational data showed a $\sim 20\%$ decrease in the α_1-CO signal with the saturation of the terminally bonded α_2-CO, no such reduction is found in the photoemission data. This is not contradictory since coverage-dependent vibrational extinction coefficients are well known in electron-energy-loss spectroscopy.[35] The UPS data imply that at these CO coverages, the α_1-CO$\rightarrow\alpha_2$-CO binding state conversion, suggested by the EELS data, is a negligible process and that the EELS result reflects a coverage-dependent vibrational cross section instead.

One observation from Figs. 6 and 8 is that the population of the α_2-CO state results in a dramatic rise in the associated 4σ peak intensity at 10.8 eV but lesser changes in the 1π and 5σ components. This can be understood by considering the expected intensity contributions from an adsorbed CO oriented along [110]. The $\theta_{lab}=42°$ experimental geometry, which includes normal emission with p-polarized light, leads to strong CO 4σ emission but is less favorable for 1π emission. Thus the observed coverage-dependent intensity behavior is reasonable for [110]-oriented α_2-CO molecules.

C. Work-function changes

Measurements of the secondary electron energy cutoff were made as a function of CO exposure to obtain the CO-induced work-function change ($\Delta\Phi$). Figure 9 is a plot of $\Delta\Phi$ versus exposure through saturation at 90 K for two independent experiments. The shaded triangle represents the sequential population of the α_2-CO molecular binding state. For exposures up to 0.8 L, corresponding to the population of the α_1-CO mode exclusively, there is a linear increase in the work function in the amount of ~ 0.2 eV. With the onset of the terminally bonded α_2-CO, however, the slope increases sharply and a further increase in Φ is found up to saturation at 3 L. This behavior is consistent with the formation of a dipole layer at the surface due to a net electron backdonation into the adsorbed carbon monoxide; similar behavior is found on other transition metals.[36] These data are plotted in Fig. 10 as a function of total CO coverage (using previously published AES data[4]) showing that the large increase in Φ is associated with a relatively small increase in Θ_{CO}; i.e., the onset of the terminally bonded α_2-CO. The induction period, during the population of the α_1-CO mode, with only a small change in work function is quite unusual for CO on a transition-metal surface.[30]

The static dipole per adsorbed CO in each of the two molecular binding states may be estimated from the approximately linear regions in Fig. 10 using[37]

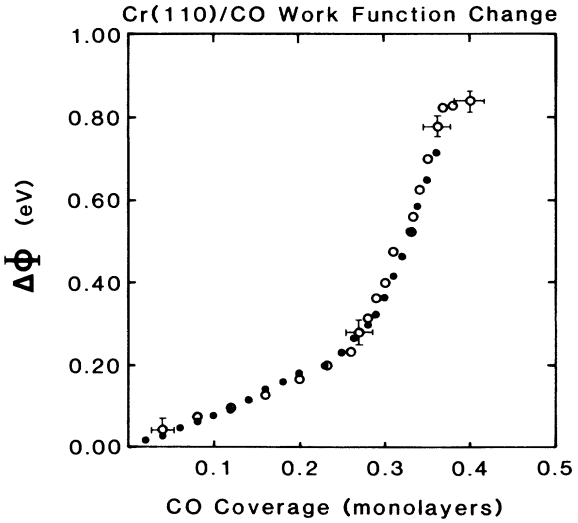

FIG. 10. Plot of work-function change vs estimated total CO coverage, using the data of Fig. 8.

$$\Delta\Phi = 2\epsilon_0 \Theta_{CO} \mu_d \ ,$$

where Φ is expressed in eV, Θ_{CO} in cm^{-2}, μ_d in Debye (1 D $=3.335\times10^{-30}$ C m), $\epsilon_0 = 3.76\times10^{-15}$ eV cm^2 D^{-1}, and the factor of 2 arises from the image dipole in the metal. For an α_1-CO coverage of 0.20 ML ($\Theta_{\alpha_1\text{-CO}} = 3.4\times10^{14}$ cm^{-2}), $\Delta\Phi \approx 0.16$ eV, and a value of $\mu_d = 0.06$ D is calculated. In contrast, using the region 0.29 ML $< \Theta_{CO} < 0.36$ ML, namely, $\Delta\Theta_{\alpha_2\text{-CO}} = 0.07$ ML, and $\Delta\Phi = 0.5$ eV, a value of $\mu_d = 0.55$ D is obtained. Within the limitations of this simplistic model, the static dipole moments per adsorbed CO molecule differ by almost an order of magnitude with binding state.

It is important to remember that these effective dipole moments are not a direct measure of the bonding dipole moment, i.e., that arising from the charge transfer alone, since (1) the above equation holds only for a continuous and infinite electric double layer, (2) the *net* dipole layer is being measured which includes the bonding dipole and non-negligible polarization effects, and (3) the calculated μ_d is linearly dependent upon the Θ_{CO} estimates. The α_1-CO molecules form islands of $c(4\times2)$ symmetry,[4] which with its large unit cell is certainly not well modeled by a continuous electric double layer. Additionally, it is possible that the saturation α_2-CO coverage at 90 K is somewhat larger than 0.10 ML, leading to an overestimation of the calculated μ_d. Without overinterpreting these data then, it is clear that the work-function changes associated with the two binding modes are also indicative of significant Cr—CO bonding differences with (apparently) less *net* charge transfer to the α_1-CO than to the terminally bonded α_2-CO *or* a smaller spatial separation of the charge in the surface dipole layer. Either explanation implies that the two molecular binding states have very different Cr—CO bonding.

D. Angular dependence

As noted previously, the present experimental arrangement is not suitable for obtaining the angular intensity distributions of CO-associated valence-band features. However, by rotating the sample manipulator, which rotates the crystal about its [1$\bar{1}$0] axis and moves the [110] azimuth in the photon plane of incidence, various coupled detection and incident photon geometries can be sampled. The purpose of this experiment is *not* to attempt to deconvolute these coupled effects in the measured angular distributions, but to (1) search all experimentally accessible geometries for changes in the CO photoemission peak intensities indicative of large matrix element effects and (2) verify the CO 4σ peak assignment.

For all accessible experimental geometries, $0° < \theta_{lab} < 100°$, the combined α_1-CO ($1\pi+5\sigma$) intensity always exceeded that of the α_1-CO 4σ peak, but the α_2-CO 4σ intensity varied significantly relative to the combined ($1\pi+5\sigma$) band. Absolute photoemission peak intensities can vary due to matrix element effects[2,3] or, more simply, changes in the CMA collection solid angle for a given θ_{lab}. Note that for $\theta_{lab} > 45°$, part of the CMA acceptance cone is obscured by the crystal itself. Hence, even in the absence of any matrix element effects (a physically unrealistic situation), the absolute peak intensities would scale with the solid angle accepted. In order to correct this, each spectrum was normalized to the SURF-II ring current, the monochromator flux at 40 eV, and then divided by the integrated inelastic electron background intensity under all of the CO UPS peaks. This correction procedure assumes an isotropic distribution of inelastic electrons in the 20–30 eV kinetic energy ($5 < E_B < 15$ eV) region. After this correction and subsequent background subtraction, differences in the CO peak intensities with θ_{lab} reflect only matrix element effects integrated over the solid angle accepted. (An invariant differential cross section would then result in no intensity change with θ_{lab}.)

The two corrected CO 4σ peak component ($E_B = 11.6$ and 10.8 eV) intensities are plotted for 1.0 and 2.0 L exposures in Figs. 11(a) and 11(b), respectively. The α_1-CO 4σ intensity distribution for a saturated α_1-CO layer, Fig. 11(a), exhibits no strong θ_{lab} dependence and uniformly weak intensity; note that the peak intensity at 11.6 eV from the 0.25 monolayer of α_1-CO is only twice that of $\sim$0.02 monolayer of the terminally bonded α_2-CO present after the 1.0 L exposure. A slight increase in the 11.6-eV intensity is seen as $\theta_{lab} \rightarrow 90°$, i.e., approaching more grazing exit angles and *s* polarization. In contrast, Fig. 11(b) demonstrates that the α_2-CO 4σ distribution (10.8-eV binding energy) is broadly peaked near $\theta_{lab} = 45°$, with strong intensity at all collection geometries. This is consistent with [110]-oriented molecules but cannot be used to definitively assign a bonding geometry. Because the 11.6 and 10.8 eV peaks overlap, the intensities for each of these spectral features are dependent upon the Gaussian decomposition procedure. Thus, the variation in the 11.6-eV data between Figs. 11(a) and 11(b) cannot be considered significant.

E. Photon-energy dependence

Resonant photoemission processes in the adsorbed carbon monoxide can be probed by exploiting the tunable radiation from SURF-II. For these experiments, a fixed

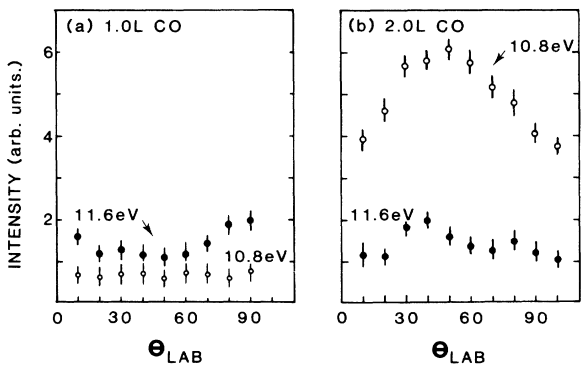

FIG. 11. Intensities of Gaussian peak components for geometry-dependent UPS data for (a) 1.0 L and (b) 2.0 L CO exposures. Spectra were normalized to SURF-II ring current, monochromator flux at $h\nu = 40$ eV, and inelastic electron background intensity under CO UPS peaks to account for variations in CMA acceptance solid angle with θ_{lab} (see text).

geometry was selected ($\theta_{lab}=42°$) and a series of UPS data was obtained as a function of photon energy for a given CO coverage. The CO 4σ shape resonance[28,29] is of interest since the resonance might be sensitive to perturbation of the CO 4σ orbital by bonding to the Cr(110) surface in the α_1-CO dissociation intermediate state. Evidence for the resonance in both binding states can be seen in both Figs. 12(a) and 12(b), with no significant change in the resonance shape being apparent. (One data point, that of $h\nu=36$ eV, is more sensitive to background subtraction due to the interference of an Auger transition with the 4σ peak.) Thus variations in the shape resonance due to Cr–CO 4σ interactions apparently are subtle, if present at all. This will be explored in greater detail in forthcoming angle-resolved UPS studies that will enable better separation of the 4σ spectral features and a more accurate measurement of the resonance.

F. CO dissociation and CO/O interactions

Annealing studies of α_1-CO and mixed adlayers using UPS showed a smooth decline of the CO valence-band features with a simultaneous growth of an O $2p$ peak at $E_B=6$ eV, following the trends of the earlier HREELS experiments.[4] Because of the overlapping CO and O valence orbitals, the UPS data are less instructive than the vibrational data and provide no new information. Work-function data are shown in Figs. 13 and 14 for the α_1-CO and mixed adlayers, respectively. The HREELS annealing studies indicate that the α_1-CO dissociation begins at ~ 150 K and is essentially complete by 250 K. Figure 13 confirms this behavior. In contrast, the dissociation of a mixed adlayer begins above ~ 170 K and is not complete until ~ 350 K (Fig. 14). The HREELS data substantiate this and indicate that a surface "Cr_xO_y" reaction species is formed during the annealing experiments. UPS data cannot provide additional, clear evidence for this species due to the coexisting CO(ads) and O(ads) surface species.

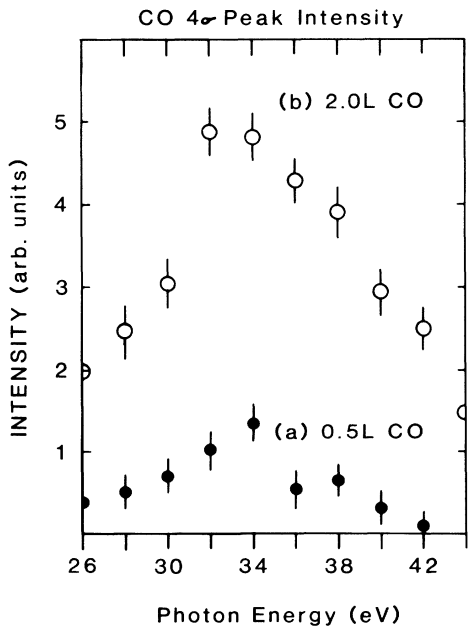

FIG. 12. CO 4σ peak intensities for (a) 0.5 L and (b) 2.0 L CO exposures as a function of photon energy.

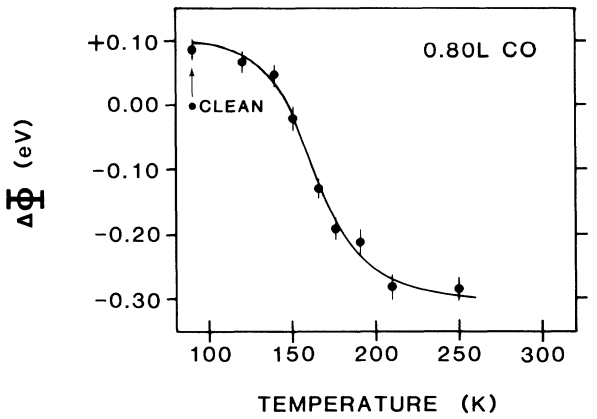

FIG. 13. Work-function change for annealing α_1-CO overlayer.

Oxygen preadsorption UPS experiments demonstrated that the total uptake of CO was reduced and the onset of the α_2-CO 4σ peak at $E_B=10.8$ eV occurred before an 0.8 L exposure; this confirms the conclusion of earlier work[21] indicating that oxygen preferentially blocks the adsorption sites for α_1-CO. Work-function data, shown in Fig. 15, show that the surface dipole layer is reduced by preadsorption of 0.5 L O_2. A comparison of the $\Delta\Phi$ versus temperature behavior in Figs. 14 and 15 indicates that CO dissociation in the mixed adlayer is more complex, possibly due to the formation of the Cr_xO_y species.

Finally, the oxygen-induced α_1-CO$\rightarrow\alpha_2$-CO binding state conversion, observed by HREELS at 120 K (Ref. 21), was demonstrated at 90 K by UPS. Figure 16 shows data for the saturated α_1-CO adlayer, followed by addition of only oxygen at 90 K. Two changes are evident in these spectra: (1) the CO 4σ intensity increases and shifts to $E_B=10.8$ eV, and (2) the O $2p$ peak appears at $E_B=6$ eV. Since no additional CO is adsorbed, these observa-

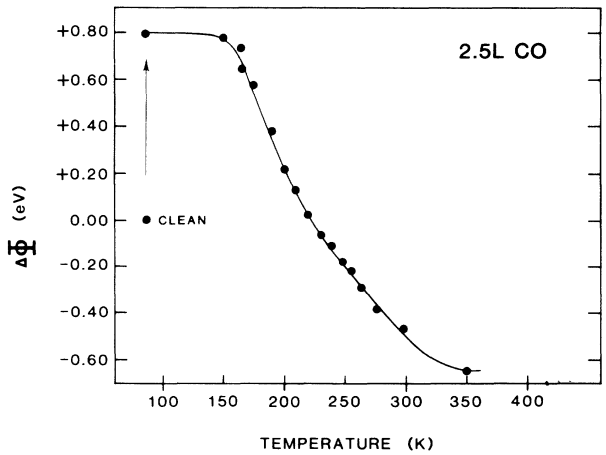

FIG. 14. Work-function change for annealing mixed α_1-CO and α_2-CO overlayers.

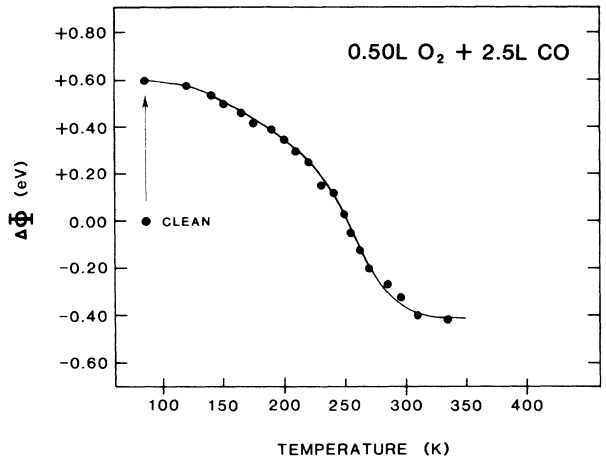

FIG. 15. Work-function change for annealing adlayer of predosed oxygen plus 2.5 L CO.

tions can only be explained by a population transfer between molecular binding states. That this process is observed at 90 K indicates that the energic barrier for this oxygen-induced site displacement and/or reorientation is small.

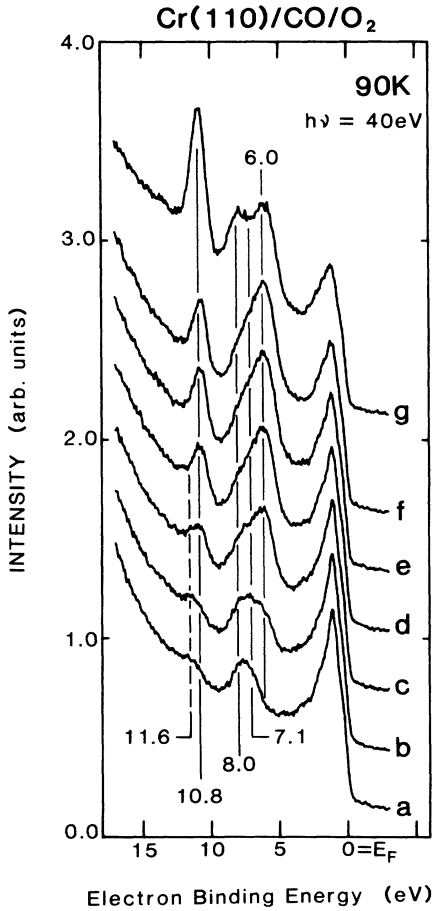

FIG. 16. UPS spectra at $\theta_{lab}=42°$, for the oxygen-induced CO binding-state conversion at 90 K. Exposures for the spectra shown are (a) 0.7 L CO followed by oxygen exposures of (b) 0.1 L, (c) 0.2 L, (d) 0.3 L, (e) 0.4 L, and (f) 0.5 L. Finally, (g) 3.0 L of CO is added to the mixed CO/O overlayer to saturate the surface with α_2-CO.

In view of the fact that adsorbed atomic oxygen does poison the Cr(110) surface for α_1-CO chemisorption, the influence of trace oxygen contamination ($\Theta \approx 2-3\%$) on the initial, "clean" surface must be considered. The most detrimental effect would be the perturbation of a very well-ordered $c(4\times2)$ α_1-CO overlayer at saturation and a slight reduction in this adlayer coverage. While any such contamination is certainly undesirable, it is not problematic at this low level. Continuing work on Cr(110) at Sandia National Laboratories has overcome this difficulty by growing pure Cr(110) crystals *in situ* for subsequent chemisorption experiments.

IV. DISCUSSION

The results presented in Secs. III B–III E for the two molecular CO adsorption states on Cr(110) reveal some similarities but more important differences. Both states are clearly chemisorbed and not physisorbed[38] or dissociated. The previously reported vibrational and stimulated desorption data suggest that the α_2-CO state consists of terminally bonded molecules oriented along [110]. All of the present UPS data are in accord with this model, which is analogous to CO on virtually every metal surface studied to date.[2,3,30] In comparison, the α_1-CO adsorption state exhibits several unusual characteristics: (1) a low-density, ordered $c(4\times2)$ overlayer at $\Theta_{\alpha_1\text{-CO}}=0.25$ ML saturation coverage, (2) atypically weak 4σ peak intensity for terminally bonded CO, although not unprecendented,[39] and (3) a greater 4σ peak width and increased 4σ binding energy ($\Delta E_B=0.8$ eV) compared to the α_2-CO state on the same surface.

The low 4σ peak intensity may be due to differential cross-section effects, reflecting a different local binding geometry which is unfavorable for 4σ signal in this experimental configuration, or simply a lower cross section overall in comparison to α_2-CO. An estimate of the order of magnitude for the latter possibility can be obtained by comparing the integrated α_1-CO and α_2-CO 4σ peak intensities at saturation (Fig. 8). The 11.6/10.8-eV ratio is 0.2 for an α_1:α_2 ratio of 2.5 ($0.25\div0.10$ ML). This means that if the two binding states consist of molecules in the same local bonding geometry (i.e., the same angular cross-section dependence), then the overall UPS cross section must be a factor of *10* greater for α_2-CO than for α_1-CO. This would certainly be a surprising result for two isostructural species on the same metal surface.

The 4σ peak width variation can be due to several factors. Since these are momentum-integrated UPS data, dispersion in the α_1-CO 4σ level could account for the slightly increased peak width for the α_1-CO. It should be noted that the α_1-CO state forms islands of $c(4\times2)$ symmetry up to saturation whereas the subsequent α_2-CO state is always disordered.[4] Based upon data for other CO-metal systems,[39–43] a 4σ bandwidth of ~0.2 eV is expected for α_1-CO in the $c(4\times2)$ overlayer where the nearest-neighbor distance is ~4 Å in the $[1\bar{1}0]$ direction. This would be consistent with the present results.

The 4σ binding-energy difference between α_1-CO and α_2-CO is the result most suggestive of different α_1-CO–Cr bonding in these UPS data. Note that the

binding-energy difference is not a coverage-dependent effect but is constant, to within ± 0.1 eV, over the entire coverage range $0 < \Theta < 0.35$ ML. In the usual description of the synergistic CO-metal bonding, the CO 5σ and 1π orbitals are perturbed from their gas-phase symmetries by the mixing with the metal valence band to form bonding-anti-bonding combinations. The occupied CO 4σ molecular orbital, being essentially a lone electron pair spatially extending from the oxygen atom,[33] is only weakly perturbed from its gas-phase character. Within this picture, it is difficult to explain an 0.8-eV difference in the binding energy of this spectator orbital. If, however, the α_1-CO dissociation intermediates are molecules in a local chemisorption geometry which permits direct metal 4σ interaction, then such a result can be understood. Calculations of CO bonding to a Cr_{33} cluster,[44] undertaken to explain the reported CO/Cr(110) vibrational data, found a 4σ binding energy increase of ~ 1 eV in going from a terminally bonded to a lying-down CO orientation. This one calculation cannot be regarded as conclusive but is consistent with the experimental observation and the models proposed earlier.

Preliminary angle-resolved UPS data[45] confirm that the α_1-CO peak intensity is significantly lower than that of α_2-CO and have measured a 4σ binding-energy difference of 0.6 eV. Surface oxygen contamination in these experiments reduced the α_1-CO coverage, as expected, and prevented a reliable measurement of the differential cross sections from being made. The angular anisotropy of CO 4σ photoemission intensity is a convenient signature of the adsorbed molecular orientation,[2] which can be deconvoluted with the appropriate differential cross-section calculations[31] or by using symmetry selection rules,[3] *if* there is only one molecular orientation for all of the electronically-indistinguishable adsorbed carbon monoxide. [It should be noted, however, that selection rule methods can be ambiguous if multiple CO orientations of different symmetry groups exist on a given surface simultaneously. This is frequently the case on high-index metal surfaces, such as Cu(311),[34] Pd(210),[46] and Pt(321).[47]] In view of the possibility that the α_1-CO 4σ orbital is more perturbed than in terminally bonded CO cases, the same care must be exercised in extracting a molecular orientation from the 4σ intensity distribution as would be used with the 5σ or 1π orbitals.

The presence of two chemically inequivalent CO binding states on Cr(110) would suggest that changes in the CO $(1\pi+5\sigma)$ binding energies might be evident as well. These angle-integrated data clearly cannot be used to identify such differences, since a spectrum such as in Fig. 7(b) would have to be fit uniquely with at least four components in the $(1\pi+5\sigma)$ manifold. A believable decomposition might be obtained from reliable angle-resolved data which do not have the momentum broadening of these angle-integrated spectra.

Recently, Cameron and Dwyer[48] have reported UPS data for the α_3-CO state on Fe(100). They observe a broad, weak "4σ" level centered at $E_B = 11.8$ eV and an increase in the density of states for $1 < E_B < 3$ eV, as is found for α_1-CO on Cr(110). Furthermore, very recent x-ray photoelectron diffraction data[49] confirm that the α_3-CO molecules on Fe(100) are tilted 55° away from the surface normal, as expected if these molecules are located in the C_{4v} hollow sites with *both* carbon and oxygen bonded to iron atoms. The similarities between the Cr(110) and Fe(100) cases, in spite of the morphological differences, strongly suggest that the UPS signature of direct metal-oxygen interaction is the CO 4σ orbital binding energy and peak intensity.

Finally, it is important to comment upon the description of these dissociation intermediates as π bonded to the surface. This may be misleading in that it suggests that the bonding contribution to the Cr—CO bond originates via the CO π system in a manner analogous to π-bonded ligands in metal complexes or the π systems of organic aromatic molecules. Even if there is extensive charge redistribution involving the CO π system by virtue of the intramolecular axis not being perpendicular to the surface, this may be more properly described as a multicentered bond involving rehybridized frontier orbitals. These detailed bonding questions will be answered as more insight is gained from realistic electronic structure calculations.

V. CONCLUSIONS

This paper presents UPS data as a function of CO coverage, detection geometry and photon energy, work-function measurements, annealing, and CO/O studies which support the following conclusions.

(1) Two sequentially populated, molecular binding modes are clearly distinguished at 90 K by the valence orbital UPS peak intensities, 4σ binding energies, 4σ peak widths (FWHM), and associated work-function changes.

(2) The α_2-CO data are consistent with those for terminally bonded CO, aligned with the [110] surface normal, bonding to Cr(110) via the accepted Blyholder model.

(3) Relative to the α_2-CO molecular binding state, the α_1-CO bonding to Cr(110) results in an atypically small surface dipole layer, a weak and broad 4σ UPS peak, and an increase of 0.8 eV in the 4σ binding energy. These observations are incompatible with a terminally bonded CO picture and supports, instead, a bonding model in which all CO frontier orbitals interact directly with Cr(110).

(4) Both molecular binding states exhibit a CO 4σ resonance at 34–36 eV photon energy. An interfering Auger transition precludes using the present data to identify small changes in this resonance structure.

(5) Annealing and CO/O studies confirm the dissociation energetics, oxygen site blocking, and oxygen-induced CO binding-state conversion (α_1-CO$\rightarrow\alpha_2$-CO) observed in previous vibrational studies.

ACKNOWLEDGMENTS

This work was supported by the Office of Naval Research, U.S. Department of Defense. Partial support

by the U.S. Department of Energy (Office of Basic Energy Sciences), under Contract No. DE-AC04-76DP00789 with Sandia National Laboratories is gratefully acknowledged. I am indebted to R. Stockbauer, R. L. Kurtz, and T. E. Madey for providing the experimental apparatus, helpful suggestions, and constructive comments, and to M. Grunze for the loan of the Cr(110) crystal.

---

*Present address.

[1] *Photoemission and the Electronic Properties of Surfaces,* edited by B. Feuerbacher, R. F. Willis, and B. Fitton (Wiley, London, 1978).

[2] N. V. Richardson and A. M. Bradshaw, in *Electron Spectroscopy: Theory, Techniques and Applications,* edited by C. R. Brundle and A. D. Baker (Academic, New York, 1981), pp. 153–196.

[3] E. W. Plummer and W. Eberhardt, Adv. Chem. Phys. **49**, 533 (1982).

[4] N. D. Shinn and T. E. Madey, Phys. Rev. Lett. **53**, 2481 (1984); J. Chem. Phys. **83**, 5928 (1985).

[5] U. Seip, M.-C. Tsai, K. Christmann, J. Küppers, and G. Ertl, Surf. Sci. **139**, 29 (1984).

[6] C. Benndorf, B. Krüger, and F. Thieme, Surf. Sci. **163**, L675 (1985).

[7] D. W. Moon, S. L. Bernasek, D. J. Dwyer, and J. L. Gland, J. Am. Chem. Soc. **107**, 4363 (1985); D. W. Moon, S. L. Bernasek, J. L. Gland, and D. J. Dwyer, Surf. Sci. **184**, 90 (1987).

[8] D. W. Moon, S. Cameron, F. Zaera, W. Eberhardt, R. Carr, S. L. Bernasek, J. L. Gland, and D. J. Dwyer, Surf. Sci. **180**, L123 (1987).

[9] F. Zaera, E. Kollin, and J. L. Gland, Chem. Phys. Lett. **121**, 464 (1985).

[10] S.-S. Sung and R. Hoffmann, J. Am. Chem. Soc. **107**, 578 (1985).

[11] G. Blyholder, J. Phys. Chem. **68**, 2772 (1963).

[12] V. Ponec, Catal. Rev. Sci. Eng. **18**, 151 (1978).

[13] E. L. Muetterties and J. Stein, J. Chem. Rev. **79**, 479 (1979).

[14] N. D. Shinn and T. E. Madey, Surf. Sci. **180**, 615 (1987).

[15] N. D. Shinn and T. E. Madey, Phys. Rev. B **33**, 1464 (1986).

[16] D. M. Hanson, R. Stockbauer, and T. E. Madey, Phys. Rev. B **24**, 5513 (1981).

[17] R. Stockbauer, D. M. Hanson, S. A. Flodström, and T. E. Madey, Phys. Rev. B **26**, 1885 (1982).

[18] S. P. Weeks and E. W. Plummer, Solid State Commun. **21**, 695 (1977).

[19] A_{eff} is estimated using the data from J. H. Weaver, C. Krafka, D. W. Lynch, and E. E. Koch, Phys. Data **19**, 55 (1981).

[20] N. D. Shinn and T. E. Madey, Surf. Sci. **173**, 379 (1986).

[21] N. D. Shinn, Langmuir **4**, 289 (1988).

[22] L. E. Davis, N. C. McDonald, P. W. Palmberg, G. E. Riach, and R. E. Weber, *Handbook of Auger Electron Spectroscopy* (Physical Electronics, Eden Prairie, Minn., 1978).

[23] J. Barth, F. Gerken, K. L. I. Kobayashi, J. H. Weaver, and B. Sonntag, J. Phys. C **13**, 1369 (1980).

[24] D. Chandesris, J. Lecante, and Y. Petroff, Phys. Rev. B **27**, 2630 (1983).

[25] H. Sugawarw, K. Naito, T. Miya, A. Kakizaki, I. Nagakura, and T. Ishii, J. Phys. Soc. Jpn. **53**, **279** (1984).

[26] D. A. Shirley, R. L. Martin, S. P. Kowalczyk, F. R. McFeely, and L. Ley, Phys. Rev. B **15**, 544 (1977).

[27] J. A. Bearden and A. F. Burr, Rev. Mod. Phys. **39**, 125 (1967).

[28] E. W. Plummer, T. Gustafsson, W. Gudat, and D. E. Eastman, Phys. Rev. A **15**, 2339 (1977).

[29] C. L. Allyn, T. Gustafsson, and E. W. Plummer, Chem. Phys. Lett. **47**, 127 (1977).

[30] See references reviewed by J. T. Yates, Jr., T. E. Madey, and J. C. Campuzano, in *The Chemical Physics of Solid Surfaces and Heterogeneous Catalysis,* edited by D. A. King and D. P. Woodruff (Elsevier, New York, 1986).

[31] J. W. Davenport, Phys. Rev. Lett. **36**, 945 (1976).

[32] H.-J. Freund and E. W. Plummer, Phys. Rev. B **23**, 4859 (1981).

[33] F. A. Cotton and G. Wilkinson, *Advanced Inorganic Chemistry,* 3rd ed. (Interscience, New York, 1972).

[34] This method was used to study selectively three distinct CO(ads) orientations on Cu(311). See, N. D. Shinn, M. Trenary, M. R. McClellan, and F. R. McFeely, J. Chem. Phys. **75**, 3142 (1981).

[35] W. Erley, H. Wagner, and H. Ibach, Surf. Sci. **80**, 612 (1979).

[36] B. E. Nieuwenhuys, Surf. Sci. **105**, 505 (1981).

[37] N. W. Ashcroft and N. D. Mermin, *Solid State Physics* (Holt, Rinehart and Winston, New York, 1976), p. 369.

[38] S. Krause, C. Mariani, K. C. Prince, and K. Horn, Surf. Sci. **138**, 305 (1984).

[39] F. Greuter, D. Heskett, and E. W. Plummer, Phys. Rev. B **27**, 7117 (1983).

[40] K. Horn, A. M. Bradshaw, and K. Jacobi, Surf. Sci. **72**, 719 (1978).

[41] K. Horn, A. M. Bradshaw, K. Hermann, and I. P. Batra, Solid State Commun. **31**, 257 (1979).

[42] E. S. Jensen and T. Rhodin, J. Vac. Sci. Technol. **18**, 470 (1981).

[43] C. W. Seabury, E. S. Jensen, and T. Rhodin, Solid State Commun. **37**, 383 (1981).

[44] S. P. Mehandru and A. B. Anderson, **169**, L281 (1986).

[45] N. D. Shinn, D. Heskett, and E. W. Plummer (unpublished).

[46] T. E. Madey, J. T. Yates, A. M. Bradshaw, and F. M. Hoffmann, Surf. Sci. **89**, 370 (1979).

[47] M. Trenary, S. L. Tang, R. J. Simonson, and F. R. McFeely, J. Chem. Phys. **80**, 477 (1984).

[48] S. D. Cameron and D. J. Dwyer, Langmuir **4**, 282 (1988).

[49] C. S. Fadley (private communication); M. Yamada, R. Saiki, G. Herman, J. Osterwalder, and C. S. Fadley (unpublished).